J Solid State Electrochem (2005) 9: 390–397
DOI 10.1007/s10008-004-0611-0

ORIGINAL PAPER

Vilmos Kertesz · Gary J. Van Berkel

Monitoring ionic adducts to elucidate reaction mechanisms: reduction of tetracyanoquinodimethane and oxidation of triphenylamine investigated using on-line electrochemistry/electrospray mass spectrometry

Received: 30 September 2004 / Revised: 14 October 2004 / Accepted: 14 October 2004 / Published online: 22 January 2005

Abstract The products of the electrochemical reduction of 7,7′,8,8′-tetracyano-*p*-quinodimethane (TCNQ) and the electrochemical oxidation of triphenylamine (TPA) were studied using a thin-layer flow cell coupled upstream on-line with electrospray mass spectrometry. Linear sweep voltammetry was used to generate intermediates and products of reduction/oxidation that were monitored by mass spectrometry in negative/positive ion mode, respectively. During reduction of TCNQ the potential dependence of the radical anion, the single-charge and the double-charge charge-transfer complexes and the double-charge anion were determined. The data provided direct evidence that following the first electron transfer practically all radical anions turn into the $[TCNQ_2^{2-} + Li^+]^-$ adduct. The adduct formation could be observed also in case of the double-charge anion, forming $[TCNQ^{2-} + Li^+]^-$ during/after the second electron transfer. Similarly, in the case of TPA the potential dependence of the radical cations of the monomer/dimer and the double-charge dimer were evaluated. Results on TPA oxidation suggested the formation of $[TPA–H]^+$ that can originate from $TPA^{\bullet+}$ by consecutive proton and electron loss. The existence of $[TPA–H]^+$ was confirmed by close inspection of the mass spectrometric peak shapes around m/z 244 and by simulation and mathematical evaluation of the measured data. However, monitoring the adducts of doubly (multiply) charged ions with oppositely charged ion(s) resulting in single-charge ions has proven to be a useful method to get relevant information about the doubly (multiply) charged ions when mass signal interference occurs between double-charge dimer and single-charge monomer molecules that have very close or equal m/z values. Moreover, in each case (reduction and oxidation) the results proved again that the electrochemistry/electrospray mass spectrometry technique is capable of monitoring reactions with complex reaction paths.

Keywords Tetracyanoquinodimethane · Triphenylamine · Electrospray mass spectrometry · Charge-transfer complex · Ion pair

V. Kertesz (✉) · G. J. Van Berkel
Organic and Biological Mass Spectrometry Group,
Chemical Sciences Division, Oak Ridge National Laboratory,
Oak Ridge, TN 37831-6131, USA
E-mail: kerteszv@ornl.gov
Tel.: +1-865-5742456
Fax: +1-865-5768559

Introduction

Electrochemistry is a convenient method to study reactions involving electron transfer. However electrochemical methods alone (e.g. cyclic voltammetry and chronoamperometry) are poor at providing direct information on the intermediate or product species. Mass spectrometric detection, which directly provides m/z, would appear to be an ideal means to investigate the products of electrochemical oxidations/reductions. On-line electrochemistry/electrospray mass spectrometry (EC/ES-MS) [1–4] has already proven successful in our hands to identify the initial polymerization products of aniline [5] and methylene blue [6], to identify the oxidation products of *N*-phenyl-1,4-phenylenediamine and benzidine [7], and to monitor the electrochemically controlled uptake and release of Cs^+ by nickel hexacyanoferrate thin-film electrodes [8]. EC/ES-MS has been used by several other groups in a variety of applications as discussed in a recent review [9].

Since its discovery in 1960 [10], tetracyanoquinodimethane (TCNQ) and its cation salts have been the subject of a large number of electrochemical and spectroscopic studies [11–35]. These studies have been motivated largely by the desire to learn ways to exploit

the conductivities of the cation salts, which are higher than those of many inorganic semiconductors. In fact, TCNQ and its cation salts have been formed into bulk electrodes, used as potentiometric sensors [36, 37] and even incorporated in electrochromic devices [38]. Despite the extensive electrochemical study, no mass spectrometric methods have been applied to provide direct evidence of the reduction products or the formation of charge-transfer complexes. Also, the presently accepted reaction mechanism [15] of the reduction of TCNQ includes the formation of double-charge anions that results in charge-decreased ion pairs with the cation(s) existing in the solution. In this paper we present mass spectrometric evidence for the potential dependence of TCNQ reaction intermediates and products. Also, we demonstrate that monitoring the mass spectrometric signal of ion pairs formed by multiply charged anions and a single-charge cation (namely Li^+) reveals information about the reduction pathway of TCNQ that would not have been available just by monitoring the signal of the double-charge anions.

Triphenylamine (TPA) also has well-characterized electrochemical behaviour [39–45]. The products of this reaction include the formation of the covalently linked double-charge dimer that overlaps in mass with the single-charge monomer in the mass spectrum. Oxidation of TPA was first examined using on-line EC/MS by Zhang and Brajter-Toth [46]. They provided direct evidence concerning the formation of the radical cation $TPA^{\bullet+}$, the radical dimer cation, i.e. tetraphenylbenzidine radical ($TPB^{\bullet+}$) and its subsequent electrochemical oxidation to the double-charge TPB^{2+}. However, they have faced the problem that signals of $TPA^{\bullet+}$ at m/z 245 and TPB^{2+} at m/z 244 overlap in the mass spectrum. Moreover, they suggested that the peak at m/z 244 originated not only from TPB^{2+} but also from $[TPA\text{-}H]^+$ that was formed by the loss of a hydrogen atom from $TPA^{\bullet+}$. To determine if the ion observed at m/z 244 was $[TPA–H]^+$ or TPB^{2+} the same group later took advantage of the high mass resolving power of Fourier transform ion cyclotron resonance MS [47]. They identified m/z 244 as consistent with $[TPA–H]^+$ under open circuit conditions and as TPB^{2+} when the cell potential was set for maximum oxidation of TPA. However, the potential dependence of these ion intensities were not fully characterized. The full potential dependence of the products of TPA oxidation is presented in this paper. Furthermore, we show that monitoring of the ion current signal of the double-charge cation/single-charge anion ion pair (namely $[TPB^{2+} + \text{triflate}^-]^+$, where triflate is trifluoromethanesulfonate) and subsequent mathematical processing of the data can distinguish between the two possible ions at m/z 244 using unit-mass resolution quadrupole based MS.

Materials and methods

TCNQ and TPA were obtained commercially (Aldrich, Milwaukee, WI, USA) and used without further purification. The solutions were prepared using acetonitrile (Burdick and Jackson, Muskegon, MI, USA) and Li triflate (99.995%, Aldrich).

All off-line cyclic voltammograms were obtained in a one-compartment electrochemical cell using a freshly polished 1.5-mm-diameter platinum working electrode (Bioanalytical Systems, BAS, West Lafayette, IN, USA), a model RE-4 Ag/AgCl/3M KCl gel reference electrode (BAS), and a platinum coil counter electrode. The potential was controlled using a CHI660 electrochemical workstation (CH Instruments, Austin, TX, USA).

The EC/ES-MS experimental setup has been described in detail elsewhere [3]. Briefly, the upstream, three-electrode, thin-layer (13-μm-thick Teflon spacing gasket between the working and the counter electrode blocks; cell volume approximately 1.0 μL) electrochemical cell was coupled on-line with a PE Sciex API 165 single quadrupole instrument (Concord, ON, Canada) using a TurboIonSpray ES ion source equipped with a 3.5-cm-long fused silica emitter capillary (330-μm outer diameter,100-μm inner diameter) [48]. The reference electrode was a model RE-4 Ag/AgCl/3M KCl gel electrode (BAS), a 6-mm-diameter platinum electrode (BAS) was used as the working electrode, and the counter electrode, constructed in-house, was made from platinum. All potentials reported regarding the work related to TCNQ are referenced to the Ag/AgCl reference electrode. A PAR model 173 potentiostat with a PAR model 175 universal programmer (Princeton Applied Research Corporation, Princeton, NJ, USA) was used to control the working electrode potential. A syringe pump (Harvard Apparatus, Cambridge, MA, USA) was used to deliver the solution through the electrochemical cell and to the ES ion source.

Simulation of the isotopic distributions of the compounds in Fig. 5 was carried out using Molecular Weight Calculator v.6.34 software [49].

Results and discussion

Reduction of TCNQ

Scheme 1 shows the accepted reaction scheme for the electrochemical reduction of TCNQ. The cyclic voltammogram in Fig. 1 clearly indicates the two consecutive, reversible electron transfer processes. Reduction of TCNQ to the stable radical anion $TCNQ^{\bullet-}$ exhibits a peak $E_{pc,1} = -0.06$ V followed by the well-separated second electron transfer at $E_{pc,2} = -0.52$ V leading to the double-charge anion, $TCNQ^{2-}$. Scheme 1 also shows that $TCNQ^{\bullet-}$ can form charge-transfer complexes with a neutral TCNQ, resulting in $TCNQ_2^{\bullet-}$, or with another $TCNQ^{\bullet-}$ molecule and a cation, that is Li^+ in our case, to form the $[TCNQ–Li–TCNQ]^-$ adduct. Figure 2 shows the mass signal intensities of $TCNQ^{\bullet-}$, $TCNQ_2^{\bullet-}$, $TCNQ^{2-}$ and single-charge Li adducts $[TCNQ–Li–TCNQ]^-$ and $[TCNQ^{2-} + Li^+]^-$, as a function of the working electrode potential during a potential scan from

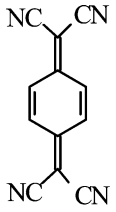

TCNQ
MW=204

$$TCNQ + e^- \rightleftharpoons TCNQ^{\bullet -} \quad (1)$$
m/z 204

$$TCNQ^{\bullet -} + TCNQ \rightleftharpoons TCNQ_2^{\bullet -} \quad (2)$$
m/z 408

$$2\,TCNQ^{\bullet -} + X^+ \rightleftharpoons [TCNQ\text{ - - }X\text{ - - }TCNQ]^- \quad (3)$$
m/z 408+MW(X^+)

$$TCNQ_2^{\bullet -} + e^- \rightleftharpoons TCNQ_2^{2-} \quad (4)$$
m/z 204

$$TCNQ_2^{2-} + X^+ \rightleftharpoons [TCNQ\text{ - - }X\text{ - - }TCNQ]^- \quad (5)$$
m/z 204 $\qquad$ m/z 408+MW(X^+)

$$TCNQ^{\bullet -} + e^- \rightleftharpoons TCNQ^{2-} \quad (6)$$
m/z 102

$$TCNQ_2^{2-} + 2e^- \rightleftharpoons 2\,TCNQ^{2-} \quad (7)$$

Scheme 1 Reactions that occur during the electrochemical reduction of tetracyanoquinodimethane (*TCNQ*)

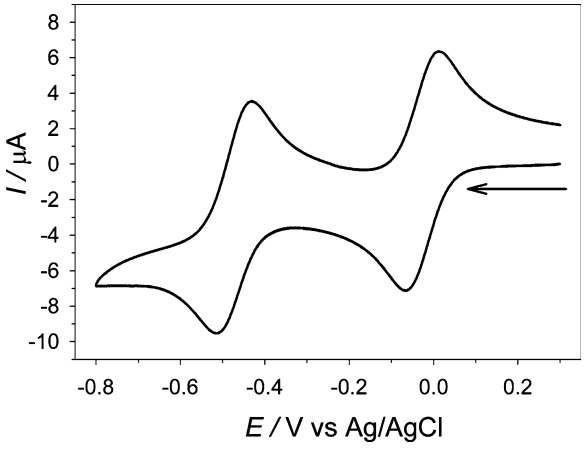

Fig. 1 Cyclic voltammogram obtained with a platinum working electrode recorded at 100 mV/s between +0.3 and −0.8 V in acetonitrile solution containing 1 mM tetracyanoquinodimethane (*TCNQ*) and 100 mM Li trifluoromethanesulfonate (triflate)

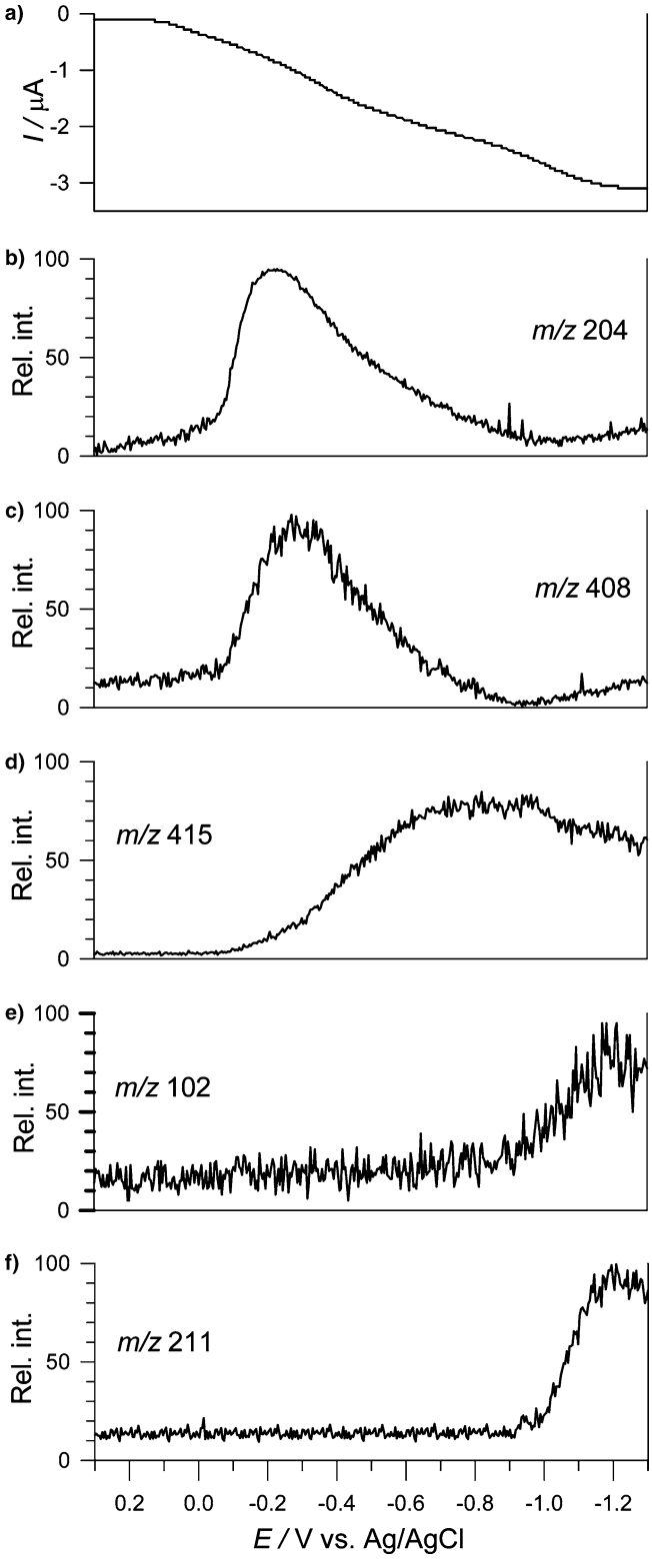

Fig. 2 Simultaneously recorded **a** current and ion current **b** m/z 204 ($TCNQ^{\bullet -}$), **c** m/z 408 ($TCNQ_2^{\bullet -}$), **d** m/z 415 ([TCNQ–Li–TCNQ]$^-$), **e** m/z 102 ($TCNQ^{2-}$) and **f** m/z 211 ($[TCNQ^{2-} + Li^+]^-$) as a function of the working electrode potential. The solution contained 100 µM TCNQ and 100 µM Li triflate in acetonitrile. All signals are normalized with respect to the signal level of the individual cations observed. Flow rate 20 µl/min. Scan rate 10 mV/s

+0.3 to −1.3 V at a scan rate of 10 mV/s. The reduction of TCNQ starts around −0.05 V as indicated in Fig. 2a and b. (The cause of the different potential values for the reduction steps between the off-line and the on-line experiments is the different solution composition. For the MS experiments, the electrolyte concentration is kept low to minimize possible gas-phase ion signal suppression. However, the lower electrolyte concentration increases the solution resistance.) In Fig. 2b, the detected amount of $TCNQ^{\bullet -}$ sharply rises from $E = -0.1$ to -0.25 V, where it reached a plateau and began to decrease at $E = -0.35$ V. The abundance of $TCNQ_2^{\bullet -}$ exhibited similar behaviour (Fig. 2c) but it reached a plateau approximately 60 mV more negative. Because $TCNQ_2^{\bullet -}$ forms in an equilibrium process from $TCNQ^{\bullet -}$ and TCNQ in a 1:1 ratio (Scheme 1), the shift in the potential can be understood in the manner that the maximum signal of $TCNQ_2^{\bullet -}$ can be achieved, where concentrations of $TCNQ^{\bullet -}$ and TCNQ are equal, which is not where the concentration of $TCNQ^{\bullet -}$ reaches its maximum. Figure 2d shows the ion current signal related to the Li-bound double-charge "dimer," $[TCNQ–Li–TCNQ]^-$ at m/z 415. Scheme 1 indicates that $[TCNQ–Li–TCNQ]^-$ can be formed in two different ways: (A) by coupling two radical anions and a lithium cation (reaction 3 in Scheme 1) or (B) by reduction of $TCNQ_2^{\bullet -}$ to $TCNQ_2^{2-}$ followed by coupling to a lithium cation (reactions 4 and 5 in Scheme 1).

Process A can be described by the following equilibrium equation:

$$K_1 = \frac{c[\mathrm{TCNQ–Li–TCNQ}]^-}{c^2_{\mathrm{TCNQ}^{\bullet -}} \cdot c_{\mathrm{Li}^+}}, \quad (1)$$

where K_1 is the equilibrium constant of process A, and $c[\mathrm{TCNQ–Li–TCNQ}]^-$, $c_{\mathrm{TCNQ}^{\bullet -}}$ and c_{Li^+} are the concentrations of $[TCNQ–Li–TCNQ]^-$, $TCNQ^{\bullet -}$ and Li^+, respectively. Equation (1) can be transformed into Eq. (2) as Li^+ concentration was constant during the experiment:

$$c_{[\mathrm{TCNQ–Li–TCNQ}]^-} = K_1' c^2_{\mathrm{TCNQ}^{\bullet -}}, \quad (2)$$

where $K_1' = K_1 c_{\mathrm{Li}^+}$. As Eq. (2) indicates, if process A was dominant, then the signal of $[TCNQ–Li–TCNQ]^-$ would correlate linearly with the square of the signal of $TCNQ^{\bullet -}$ exhibiting a similar maximum-type curve as the plot in Fig. 2b. This was not the case. If process B was the dominant reaction, then the intensity of $TCNQ_2^{\bullet -}$ at m/z 408 should have decreased to zero, while that at m/z 415 representing $[TCNQ–Li–TCNQ]^-$ should have increased and reached a maximum as the potential became more negative. The ion signals in Fig. 2c and d follow this pattern, confirming that process B dominates. Figure 2e and f shows the concentration profile of the double-charge $TCNQ^{2-}$ and its Li adduct ($[TCNQ^{2-} + Li^+]^-$) as a function of the working electrode potential. Production of the dimer anion starts around $E = -1$ V and the two curves move together. Each of them indicates, directly in Fig. 2e and indirectly in Fig. 2f, the concentration of the same dimer anion. Also, the decrease in the signal intensity of m/z 415 representing $[TCNQ–Li–TCNQ]^-$ at more negative potentials than $E = -1.0$ V in Fig. 2d is due to reduction that results in the dimer anion.

Oxidation of TPA

Scheme 2 shows the oxidation pathway of TPA. As a first step, the oxidation of TPA generates a radical cation in a one-electron transfer process ($TPA^{\bullet +}$, m/z 245) followed by the dimerization of the generated radicals resulting in TPB ($M_r = 488$). Previous ES/MS studies [47] have also shown the formation of an ion corresponding to $[TPA–H]^+$ at m/z 244. Formation of this species was explained as hydrogen radical loss from the radical cation. Since the dimer is easier to oxidize than the monomer, the TPB formed immediately undergoes two discrete one-electron oxidation steps [39–45] resulting in $TPB^{\bullet +}$ with m/z 488 as an intermediate and TPB^{2+} at m/z 244 as the final oxidation product. The cyclic voltammogram of TPA in Fig. 3 reflects this

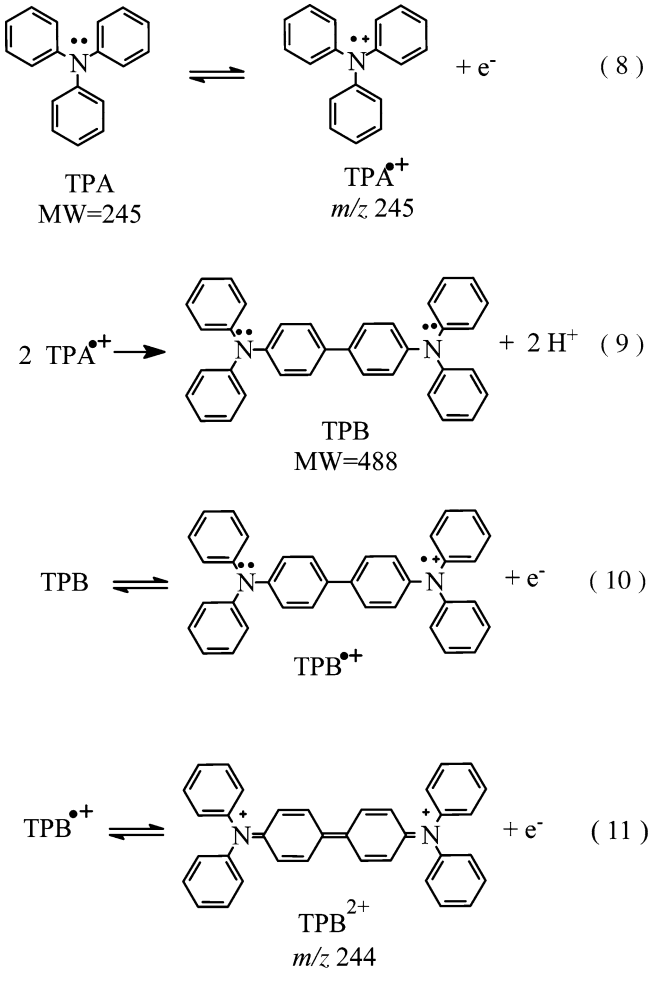

Scheme 2 Oxidation pathway of triphenylamine (*TPA*)

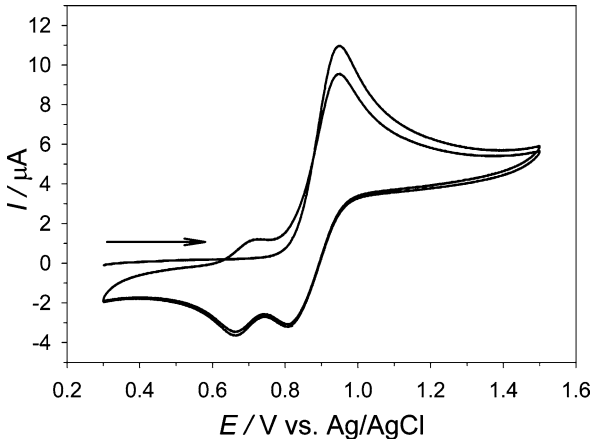

Fig. 3 The first two cyclic voltammograms obtained with a platinum working electrode recorded at 100 mV/s between −0.3 and +1.5 V in acetonitrile solution containing 1 mM triphenylamine (*TPA*) and 100 mM Li triflate

reaction path. The first anodic half-cycle does not exhibit peaks up to +0.8 V. At $E_{pa,2} = +0.95$ V a large oxidation peak is observed owing to the oxidation of the monomer and the follow-up oxidation of the dimer molecules. On the cathodic half-cycle two discrete peaks were observed at $E_{pc,1} = +0.83$ V and $E_{pc,2} = +0.66$ V owing to the two discrete one-electron reduction step of TPB^{2+}. On the second anodic half-cycle the one-electron oxidation of the reduced TPB to $TPB^{\bullet+}$ resulted in a peak at $E_{pa,1} = +0.72$ V.

Figure 4 shows the mass signal intensities of ions $TPA^{\bullet+}$, $TPB^{\bullet+}$, TPB^{2+} (or/and $[TPA\text{-}H]^{+}$) and the triflate adduct of TPB^{2+} ($[TPB^{2+} + triflate^{-}]^{+}$) recorded during a potential scan from +0.8 to +1.4 V at scan rate of 2 mV/s. The dashed lines indicate the potential values at half signal levels (HSL) for the different ions, except that of *m*/*z* 244 (see later). The oxidation of TPA starts at around +0.9 to +0.95 V as indicated by the current and the ion intensity of $TPA^{\bullet+}$ in Fig. 4a and b, respectively. The amount of $TPA^{\bullet+}$ detected increases with the potential and reaches its HSL and maximum at around +1.01 and +1.15 V, respectively. Based on the oxidation scheme, the dimer is produced in the follow-up chemical step that is subsequently oxidized to $TPB^{\bullet+}$ and is observed at *m*/*z* 488. Figure 4c reveals that the signal of $TPB^{\bullet+}$ reaches its HSL and maximum at around +1.06 and +1.2 V, respectively. The difference in the corresponding HSL potential values of $TPA^{\bullet+}$ and $TPB^{\bullet+}$ is indicative of the follow-up chemical reaction of $TPA^{\bullet+}$. On the basis of the potential dependence of the $TPB^{\bullet+}$ intermediate in Fig. 4c, the shape of the *m*/*z* 244 versus potential curve in Fig. 4d (i.e. the rise of the signal at around the same potential values where $TPA^{\bullet+}$ was generated in Fig. 4b) cannot be explained with the formation of TPB^{2+} alone. TPB^{2+} is a product of the one-electron oxidation of $TPB^{\bullet+}$, consequently it should start to rise at the same or a more positive potential than the signal of $TPB^{\bullet+}$. Equation

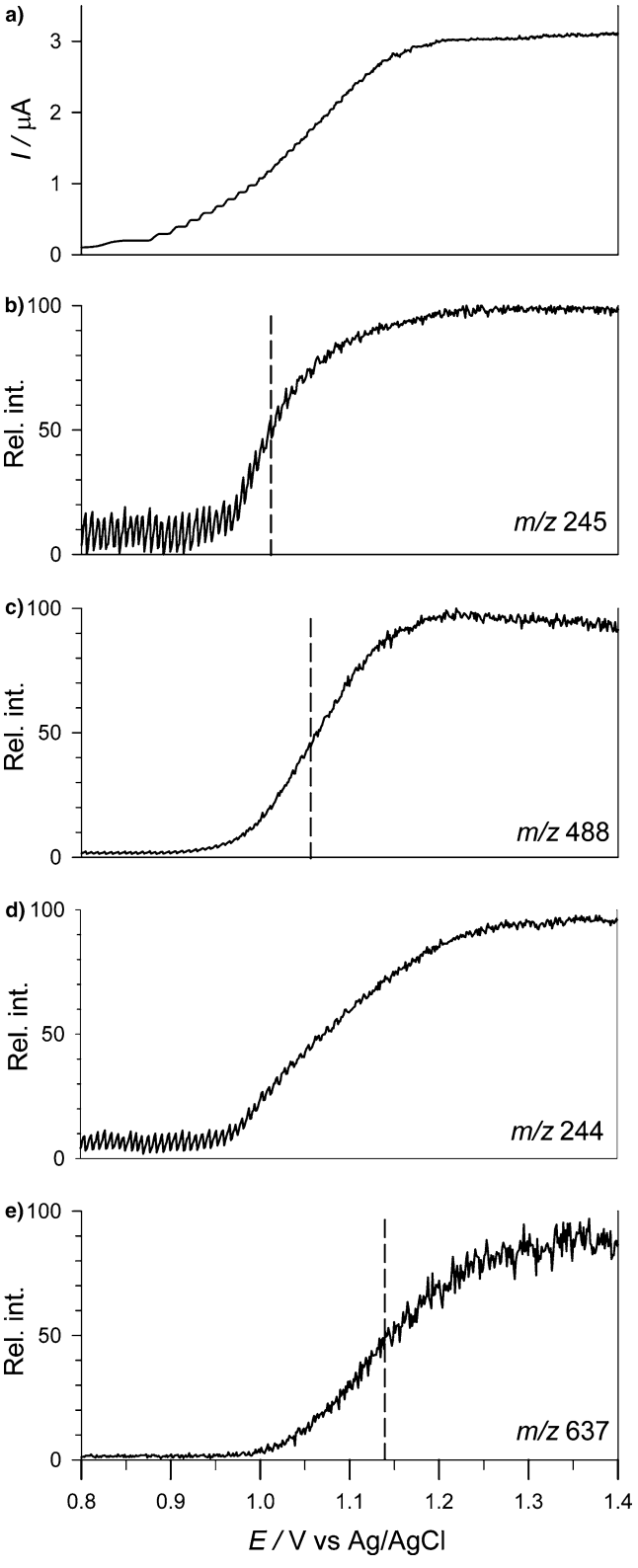

Fig. 4 Simultaneously recorded **a** current and ion current at **b** *m*/*z* 245 ($TPA^{\bullet+}$), **c** *m*/*z* 488 ($TPB^{\bullet+}$), **d** *m*/*z* 244 ($[TPA\text{–}H]^{+}$ and/or TPB^{2+}) and **e** *m*/*z* 637 ($[TPB^{2+} + triflate^{-}]^{+}$) as a function of the working electrode potential. The solution contained 50 µM TPA and 1 mM Li triflate in acetonitrile. All signals are normalized with respect to the signal level of the individual cations observed. Flow rate 20 µl/min. Scan rate 2 mV/s

(3) describes the concentration dependence between $[TPB^{2+} + triflate^-]^+$ and TPB^{2+}:

$$K_2 = \frac{c_{[TPB^{2+}-triflate^-]^+}}{c_{TPB^{2+}} c_{triflate^-}}, \quad (3)$$

where K_2 is the equilibrium constant, and $c_{[TPB^{2+}-triflate^-]^+}$, $c_{TPB^{2+}}$ and $c_{triflate^-}$ are the concentrations of $[TPB^{2+} + triflate^-]^+$, TPB^{2+} and $triflate^-$, respectively. Equation (3) can be transformed into Eq. (4) as the $triflate^-$ concentration was constant during the experiment:

$$c_{[TPB^{2+}-triflate^-]^+} = K_2' c_{TPB^{2+}}, \quad (4)$$

where $K_2' = K_2 c_{triflate^-}$. Figure 4e shows the potential dependence of the ion current signal of the $[TPB^{2+} + triflate^-]^+$ adduct. Equation (4) shows that the $[TPB^{2+} + triflate^-]^+$ adduct and TPB^{2+} should maintain a constant concentration ratio over the potential range examined, i.e. the potential dependence profile of $[TPB^{2+} + triflate^-]^+$ should follow that of TPB^{2+}. To test this, the normalized curve indicating the difference between ion signals of m/z 244 and m/z 637 was plotted (Fig. 5). This plot was constructed by first subtracting the normalized intensity of m/z 637 in Fig. 4e from that of m/z 244 in Fig. 4d. If normalized signals of m/z 244 and m/z 637 originated from the same molecule then no change would be expected in their normalized signal levels as a function of potential. As Fig. 5 reveals, the "difference curve" has a peak shape with a maximum of around 27% intensity difference between the two original normalized signals. This result indicates that the species detected at m/z 244 was not exclusively TPB^{2+}. The other component is probably $[TPA–H]^+$ as was reported by Zhang and coworkers [46, 47]. Figure 5 also reveals the potential dependence on the formation of $[TPA–H]^+$.

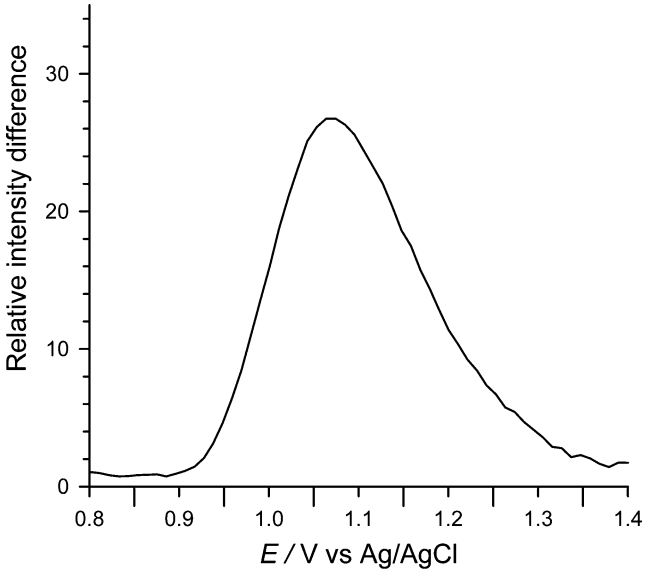

Fig. 5 Difference curve between normalized signal intensities of m/z 244 and m/z 637. The plot was constructed by subtracting the normalized intensity of m/z 637 (Fig. 4e) from the normalized intensity of m/z 244 (Fig. 4d) and normalized again to its maximum. Conditions are the same as in Fig. 4

Another approach to differentiate between $[TPA–H]^+$ and TPB^{2+} is to record the mass spectrum at a potential where each of the ions should exist and to compare the measured spectrum against the simulated mass spectrum assuming that $[TPA–H]^+$ or TPB^{2+} generates 100% of the peak at m/z 244. As TPB^{2+} is a double-charge ion, its isotopic peak at one mass unit higher would result in a peak at m/z 244.5. In the case of $[TPA–H]^+$ this peak is not expected.

In Fig. 6a the mass spectrum was recorded at $E = +1.0$ V. The mass spectrometer was tuned for baseline separation in the m/z range examined for single-charge ions. Figure 6a reveals that some overlap existed between the peaks at m/z 244 and m/z 245. Figure 6b shows the calculated mass spectrum, where the peaks at m/z 244 and at m/z 245 each originated from single-charge ions. Moreover, the ratio of the intensity of the two ions was set to produce the same peak height ratio for m/z 244 and m/z 245 as was measured in Fig. 6a to make the comparison between measured and simulated curves easier. Similarly, Fig. 6c shows the calculated mass spectrum, where the peak at m/z 244 originated from a double-charge ion (peak at m/z 245 was simulated as the single-charge species, i.e. $TPA^{\bullet+}$).

Comparison of the overlap between m/z 244 and m/z 245 in Fig. 6b and c reveals that the peak at m/z 244 on the measured curve in Fig. 6a is a mixture of single- and double-charge ions, i.e. $[TPA–H]^+$ and TPB^{2+}, which is the same conclusion drawn from inspection of Fig. 5. However, the reaction in which $[TPA–H]^+$ is formed may not be the radical hydrogen loss from $TPA^{\bullet+}$ proposed by Zhang and coworkers [46, 47]. One possibility would be to produce $[TPA–H]^+$ by proton loss from the double-charge monomer TPA^{2+}. Proton loss from double-charge ions is a well-known follow-up chemical reaction [50] and has been shown by on-line EC/ES-MS, e.g. in the case of β-carotene [2]. We monitored the intensity of m/z 122.5 and m/z 393 that would have been direct evidence for the existence of TPA^{2+} and $[TPA^{2+} + triflate^-]^+$, respectively, but no diagnostic signals were detected (not shown). The inability to detect TPA^{2+} may be the result of the fast proton-loss follow-up chemical reaction. These types of fast follow-up reactions cannot be followed using an upstream cell, where it takes several seconds to get the analyte exiting the cell to reach the mass spectrometer (the flow rate must have been kept relatively low for high oxidation efficiency). Also, until now no electrochemical evidence was provided for the existence of TPA^{2+} as its formation is not a thermodynamically favoured process. The other possibility to form $[TPA–H]^+$ is the consecutive proton and electron loss of $TPA^{\bullet+}$ demonstrated by reactions 12 and 13 in Scheme 3. Reaction 12 includes a route to produce the neutral radical form of [TPA–H] that results in $[TPA–H]^+$ in a following one-electron

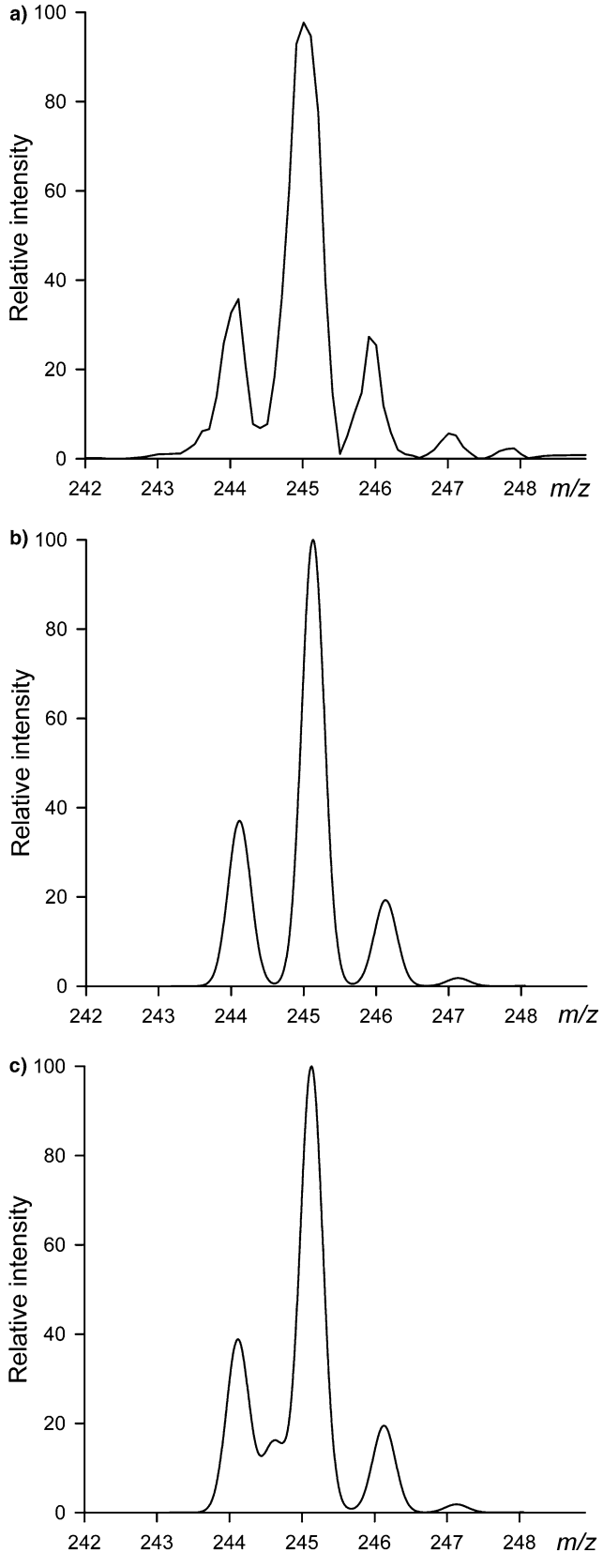

oxidation step. Furthermore, the structure of [TPA–H] suggests that this compound could undergo a radical dimerization reaction to form TPB. However, this dimerization route has never been evaluated but it is another possible pathway based on the presence of $[TPA–H]^+$.

Fig. 6 **a** Measured, background subtracted, averaged electrospray mass spectrum of 50 μM TPA and 1 mM Litri flate in acetonitrile at $E = +1.0$ V working electrode potential. Flow rate 20 μl/min. **b** Simulated mass spectrum that represents the summarized signal of $TPA^{\bullet+}$ and $[TPA–H]^+$ in a 1:0.36 ratio to get the same m/z 244:m/z 245 signal ratio that is in Fig. 5a. **c** Simulated mass spectrum that represents the summarized signal of $TPA^{\bullet+}$ and TPB^{2+} in a 1:0.36 ratio to get the same m/z 244:m/z 245 signal ratio that is in Fig. 5a

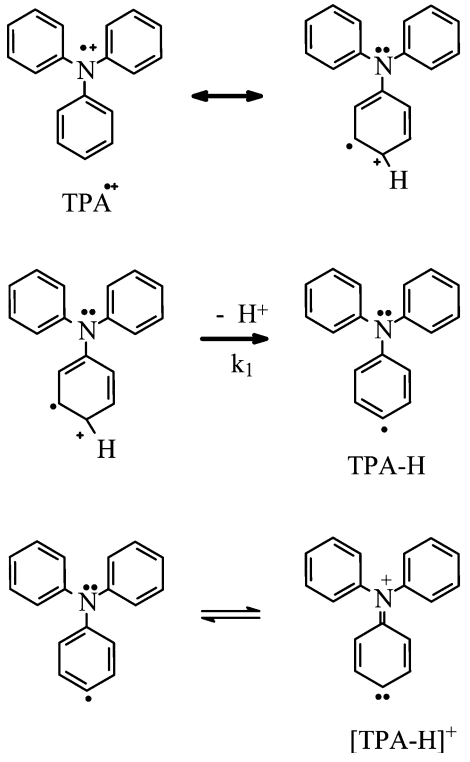

(12)

(13)

Scheme 3 Resonance structures and a possible mechanism to form $[TPA–H]^+$ from $TPA^{\bullet+}$

Conclusions

In this work, the products of the electrochemical reduction of TCNQ and the electrochemical oxidation of TPA were investigated using on-line EC/ES-MS. The study of TCNQ reduction has revealed the potential dependence of the radical anion, the single-charge and the double-charge charge-transfer complexes and the double-charge anion. The results presented provide direct evidence for the nearly exclusive presence of the $[TCNQ–Li–TCNQ]^-$ adduct after the first reduction step has been completed. The adduct formation was also detected after the second electron transfer resulting in the single-charge ion of $[TCNQ^{2-} + Li^+]^-$. The potential dependence of the radical cations of the monomer/dimer and the double-charge dimer during oxidation of TPA

was also investigated. The results indicated the formation of $[TPA–H]^+$ which interfered with the mass signal of TPB^{2+}. Again, monitoring the mass spectrometric signal of an adduct, namely $[TPB^{2+} + triflate^-]^+$ together with mathematical post-processing of the data has proven to be a fruitful technique to get information in the case of interfering single- and double-charge ions in the mass spectrum using a simple single-quadrupole mass spectrometer. In the future, we plan to investigate the existence of possible adducts of $[TPA–H]^+$ and possible short-lived intermediates of TPA oxidation with a controlled-potential electrochemical emitter cell system [51]. With this cell the products of the electrochemical reaction can take a very short time, around 100 ms, to reach the gas phase in the mass spectrometer.

The results presented here also demonstrate that the EC/ES-MS technique is a highly informative tool in the study of the products of electrochemical processes and that it should prove very helpful in the identification of unidentified products of other electrode reactions.

Acknowledgements ES-MS instrumentation was provided through a Cooperative Research and Development Agreement with MDS SCIEX (CRADA no. ORNL02-0662). V.K. acknowledges an ORNL appointment through the ORNL Postdoctoral Research Associates Program. The work carried out at ORNL was supported by the Division of Chemical Sciences, Geosciences, and Biosciences, Office of Basic Energy Sciences, United States Department of Energy under contract DE-AC05-00OR22725 with ORNL, managed and operated by UT-Battelle, LLC.

References

1. Deng H, Van Berkel GJ (1999) Electroanalysis 11:857
2. Zhou F, Van Berkel GJ (1995) Anal Chem 67:3643
3. Pretty JR, Van Berkel GJ (1998) Rapid Commun Mass Spectrom 12:1644
4. Pretty JR, Deng H, Goeringer DE, Van Berkel GJ (2000) Anal Chem 72:2066
5. Deng H, Van Berkel GJ (1999) Anal Chem 71:4284
6. Kertesz V, Van Berkel GJ (2001) Electroanalysis 13(17):1425
7. Kertesz V, Deng HT, Asano KG, Hettich RL, Van Berkel GJ (2002) Electroanalysis 14:1027
8. Kertesz V, Dunn NM, Van Berkel GJ (2002) Electrochim Acta 47(7):1035
9. Karst U (2004) Angew Chem Int Ed 43:2476
10. Kepler RG, Bierstedt E, Merrifield RE (1960) Phys Rev Lett 5:503
11. Suchanski MR, Van Duyne RP (1976) J Am Chem Soc 98:250
12. Larsen H, Pedersen SU, Pedersen JA, Lund H (1992) J Electroanal Chem 331:971
13. Watanabe M, Wooster TT, Murray RW (1991) J Phys Chem 95:4573
14. Inzelt G, Day RW, Kinstle JF, Chambers JQ (1983) J Phys Chem 87:4592
15. Inzelt G (1994) Mechanism of charge transport in polymer-modified electrodes. In: Bard AJ (ed) Electroanalytical chemistry, vol 18. Marcel Dekker, New York, pp 89–241
16. Francis CV, Joo P, Chambers JQ (1987) J Phys Chem 91:6315
17. Khatkale MS, Devlin JP (1979) J Chem Phys 70:1851
18. Miller JS, Ohare DM, Chakraborty A, Epstein AJ (1989) J Am Chem Soc 111:7853
19. Terashita S, Ozaki Y, Iriyama K (1993) J Phys Chem 97:10445
20. Martin N, Behnisch R, Hanack M (1989) J Org Chem 54:2563
21. Kini AM, Cowan DO, Gerson F, Mockel R (1985) J Am Chem Soc 107:556
22. Wheland RC, Gillson JL (1976) J Am Chem Soc 98:3916
23. Jaeger CD, Bard AJ (1979) J Am Chem Soc 101:1690
24. Hurditch RJ, Vincent VM, Wright JD (1972) J Chem Soc Faraday Trans 1, 68:465
25. Melby LR, Harder RJ, Hertler WR, Mahler W, Benson RE, Mochel WE (1962) J Am Chem Soc 84:3374
26. Day RW, Inzelt G, Kinstle JF, Chambers JQ (1982) J Am Chem Soc 104:6804
27. Inzelt G, Day RW, Kinstle JF, Chambers JQ (1984) J Electroanal Chem 161:1475
28. Inzelt G, Chambers JQ, Kinstle JF, Day RW (1984) J Am Chem Soc 106:3396
29. Inzelt G, Chambers JQ, Kinstle JF, Day RW, Lange MA (1984) Anal Chem 56:301
30. Inzelt G, Chambers JQ, Bacskai J, Day RW (1986) J Electroanal Chem 201:301
31. Inzelt G, Horanyi G, Chambers JQ, Day RW (1987) J Electroanal Chem 218:297
32. Inzelt G, Horanyi G, Chambers JQ (1987) Electrochim Acta 32:757
33. Inzelt G, Szabo L, Chambers JQ, Day RW (1988) J Electroanal Chem 242:265
34. Inzelt G (1990) J Electroanal Chem 287:171
35. Bellec V, De Backer MG, Levillain E (2001) Electrochem Commun 3(9):483
36. Ruzicka J, Lamm CG (1971) Anal Chim Acta 54:1
37. Sharp M (1976) Anal Chim Acta 85:17
38. Yasuda A, Seto J (1988) J Electroanal Chem 247:193
39. Seo ET, Nelson RF, Fritsch JM, Marcoux LS, Leedy DW, Adams RN (1966) J Am Chem Soc 88:3498
40. Nelson RF, Adams RN (1968) J Am Chem Soc 90:3925
41. Marcoux LS, Adams RN, Feldberg SW (1969) J Phys Chem 73:2611
42. Nelson RF, Feldberg SW (1969) J Phys Chem 73:2623
43. Nelson RF, Philip RH Jr (1979) J Phys Chem 83:713
44. Oyama M, Nozaki K, Okazaki S (1979) Anal Chem 63:1387
45. Sumiyoshi T (1995) Chem Lett 645
46. Zhang T, Brajter-Toth A (2000) Anal Chem 72:2533
47. Zhang T, Palii SP, Eyler JR, Brajter-Toth A (2002) Anal Chem 74:1097
48. Kertesz V, Van Berkel GJ (2001) J Mass Spectrom 36(2):204
49. Monroe M (2004) Molecular Weight Calculator 6.34. (This molecular weight and isotope calculation program can be downloaded from the Internet.) Web-address: http://www.geocities.com/alchemistmatt/
50. Yoshida K (1984) Electrooxidation in organic chemistry. Wiley, New York.
51. Van Berkel GJ, Asano KG, Granger MC (2004) Anal Chem 76(5):1493